Comparison between a multiple scattering method and direct numerical simulations for elastic wave propagation in concrete

M. Chekroun[1,2], L. Le Marrec[3], B. Lombard[4], J. Piraux[4], and O. Abraham[1]

Abstract Numerical simulations are performed to study the propagation of elastic waves in a 2-D random heterogeneous medium such as concrete. To reduce spurious numerical artefacts to a negligible level, a fourth-order time-domain numerical scheme and an immersed interface method are used together. Effective properties of the equivalent homogeneous medium are extracted and compared to the predictions of a multiple scattering method (ISA), to evaluate the validity of this latter.

1 Introduction

Concrete is made up of coarse aggregates embedded in a cement paste matrix (mortar). When ultrasounds propagate in this heterogeneous medium, multiple scattering is important when the wavelength and the size of scatterers are similar. In this case, the wave field is the superposition of a coherent field, obtained by averaging fields over several realizations of disorder, and of an incoherent field. The coherent field amounts to waves propagating in an equivalent homogeneous medium, with effective phase velocity and attenuation deduced from an effective wavenumber.

The goal of multiple-scattering methods, such as the Independent Scattering Approximation (ISA) [1], is to provide analytical expressions of this effective wavenumber. A basic assumption for derivation of ISA is that the concentration of scatterers is low. Since aggregates may represent 50 % in volume, the medium cannot be considered as dilute, and a deeper analysis is required to decide whether ISA is valid in that case.

(1) LCPC centre de Nantes - BP4129, 44341 Bouguenais, France
e-mail: mathieu.chekroun@lcpc.fr
(2) Électricité de France (EDF R&D) - BP49, 78401 Chatou cedex, France
(3) IRMAR - Université Rennes 1, Campus Beaulieu - 35042 Rennes, France
(1) LMA - CNRS, 31 chemin Joseph Aiguier - 13402 Marseille, France.

For that purpose, a purely numerical methodology is followed, based on 2D direct numerical simulations and on signal-processing tools. Doing so is much faster and less expensive than real experiments, allowing also much finer measures. In previous works, this methodology has been applied successfully to a case where ISA has been experimentally validated: steel rods immersed in water [2]. In the present paper, the host medium and the aggregates are both modeled as elastic media. Cases of different concentrations of aggregates are discussed. Since the propagation of Rayleigh waves along a free surface of concrete is the original motivation of the present study, the case of both compressional and shear incident plane wave is considered (P-SV problem).

2 Problem statement

2.1 Concrete model

Aggregates are assumed to be circular cylinders with a unique radius $a = 6$ mm, in a bidimensional geometry. The probing frequency varies from 50 kHz to 700 kHz. In that range, wavelengths vary from about 3 mm (S wave) to 90 mm (P wave), hence aggregates are considered as heterogeneities for waves. On the contrary, mortar is considered as an homogeneous medium for wave propagation, since the size of its components (water, sand and cement) is much smaller than the wavelengths. The concrete is then be considered as a two phase medium with parameters [3]

$$(\rho, c_p, c_s) = \begin{cases} (2050\,\mathrm{kg/m^3}, 3950\,\mathrm{m/s}, 2250\mathrm{m/s}) & \text{in mortar,} \\ (2610\,\mathrm{kg/m^3}, 4300\,\mathrm{m/s}, 2475\mathrm{m/s}) & \text{in aggregates,} \end{cases}$$

where ρ is the density, c_p and c_s are the celerities of P and S waves. The concentration of aggregates in concrete is described by the number n of scatterer per unit area. Three surface ratios $\phi = n\pi a^2$ are considered in the following: $\phi = 6\%$, 12%, and 18%, defining 3 concretes called C6, C12 and C18 respectively. The average distance between nearest scatterers is $l_\phi = a\sqrt{\pi/\phi}$, hence: $l_{6\%} = 43$ mm, $l_{12\%} = 32$ mm, $l_{18\%} = 25$ mm. We assume perfect contact between aggregates and mortar (continuity of tractions and of displacements at the boundaries) and no dissipative effect. These hypotheses and the low density of aggregates affect the realism of our model but allow us to focus on the validity of ISA without additional artifact.

2.2 Independent Scattering Approximation

The formulation of the *Independent Scattering Approximation* (ISA) is usually established with an fluid matrix [4], but it can be straightforwardly extended to an

elastic matrix. As correlation between scatterers is not taken into account, mode conversion does not perturb the expression of effective wavenumbers. Then, the effective wavenumbers $k_{P,eff}$ and $k_{S,eff}$ obtained with incident plane P and S waves satisfy

$$k_{P,eff}^2(\omega) = k_{P,0}^2 - 4in\, f_{PP}(0), \qquad k_{S,eff}^2(\omega) = k_{S,0}^2 - 4in\, f_{SS}(0), \tag{1}$$

where $k_{P,0}$ and $k_{S,0}$ denote P and S wavenumbers of the matrix, $\omega = 2\pi f$ is the angular frequency, and $f_{PP}(0)$ is the far field pattern in P mode of the interaction between an incident plane P wave and a single scatterer in the forward direction (idem for S waves with $f_{SS}(0)$).

3 Direct numerical simulation

3.1 Elastodynamic equations

A velocity-stress formulation of 2D elastodynamics is followed. To solve the hyperbolic system so-obtained, a uniform Cartesian grid with mesh sizes $\Delta x = \Delta y$ and time step Δt is defined. An explicit fourth-order accurate finite-difference ADER scheme is used [5], with a CFL constraint of stability $\beta = c\Delta t/\Delta x \leq 0.9$. A plane wave analysis of this scheme is performed in homogeneous medium, in terms of β and of $G = \Delta x/\lambda$, $G \in]0, 0.5]$, where λ is the wavelength [6]. The maximal artifacts are obtained when the direction of propagation coincides with grid axes, that is in 1D configurations. In that case, the ratio q between exact and discrete phase velocities, and the discrete attenuation α, are

$$q(\beta, G) = 1 - \frac{2\pi^4}{15}(\beta^2 - 1)(\beta^2 - 4)G^4 + O(G^6). \tag{2}$$

$$\alpha(\beta, G, \Delta x) = \frac{4\pi^6\beta}{9\Delta x}(\beta^2 - 1)(\beta^2 - 4)G^6 + O(G^8). \tag{3}$$

In forthcoming numerical experiments, $\beta = 0.44$ and $G = 1/90$ correspond to the most penalizing situation of SV waves in mortar at $f = 250$ kHz. With these parameters, (3) gives a quality factor $Q \approx 3.2\,10^7$, hence the numerical attenuation is much smaller than the expected physical attenuation of the effective medium.

3.2 Discretization of interfaces

Three classes of drawbacks are classically induced by interfaces in finite-difference schemes on Cartesian grids. First, the geometrical description of arbitrary-shaped interfaces is poor, and generates spurious diffractions. Second, the jump conditions

are not enforced numerically. Third and last, non-smoothness of the solution across interfaces decreases the accuracy, leading to spurious oscillations or even instabilities. These three drawbacks prevent from using simulations as metrological tools in highly heterogeneous media. To circumvent them, the ADER scheme is coupled with an immersed interface method [7], which accounts both for the jump conditions and for the subcell geometry at points along the interfaces. The main part of the work can be done during a preprocessing step, before numerical integration. At each time step, $O(\mathscr{L}/\Delta x)$ matrix-vector products are done, where $\mathscr{L}$ is the total perimeter of interfaces, and the matrices are small-size, typically 5×100. Then, the results are injected in the scheme.

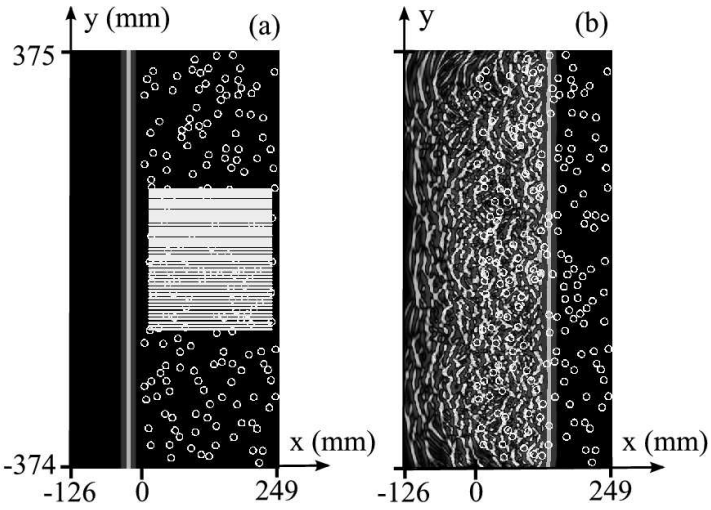

Fig. 1 Snapshot of the horizontal velocity at the initial instant (a), and after 0.04 μs of propagation (b). In (a), the regular grid denotes the location of the receivers.

3.3 Numerical setup

The size of the computational domain is 375 mm along x and 750 mm along y, with $\Delta x = 0.1$ mm and $\beta = 0.85$ in aggregates. The aggregates are randomly distributed on a 248 mm $\times$ 740 mm rectangular subdomain (figure 1). An exclusion length of $6\Delta x$ between each scatterer is ensured. The right-going incident P or SV plane wave is a Ricker centered at 250 kHz. At the initial instant, the right part of the wave front is located at $x = 0$. At each time step, the exact plane wave solution in homogeneous medium is enforced on the edges of the domain. The simulations are stopped when the incident wave has crossed the inclusions: 3250 time steps with an incident P wave, 5300 time steps with an incident S wave.

A set of 41 horizontal lines of receivers is taken with $N = 221$ regular offsets along x, denoted by $d_i = d_0 + i\Delta x_r$, with $i = 0, ..., N-1$, $d_0 = 14$ mm and $\Delta x_r = 1$ mm. The distance between two lines is $\Delta y_r = 6.25$ mm. Each line corresponds to a realization of a random process. These parameters are discussed in section 4.2. Receivers are sufficiently far from the boundaries of the computational domain to avoid spurious reflections.

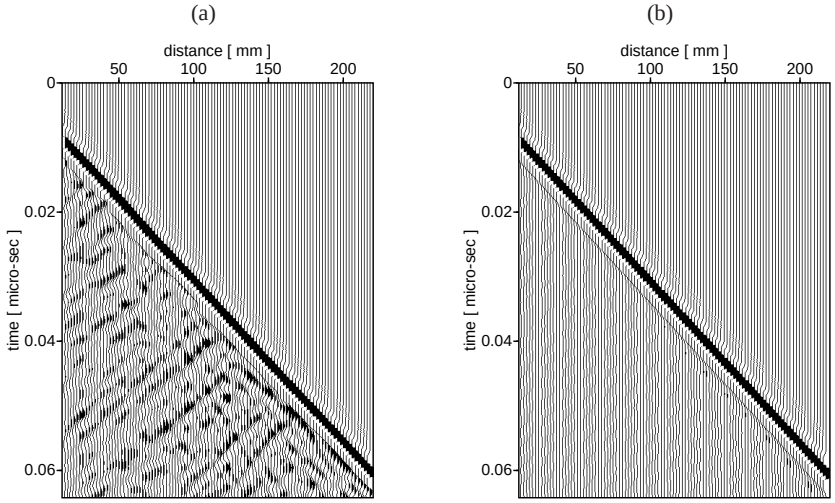

Fig. 2 Seismograms of the horizontal velocities u_x from the simulation with incident P wave in C12: one particular realization (a), coherent field obtained after averaging (b).

Three simulations provide $41 \times 3 = 123$ independent realizations of disorder, ensuring the convergence of the signal processing methods. Recorded velocities along a line of receivers can be plotted as seismograms. A particular seismogram in the case of incident P wave in C12 is presented in figure 2(a). A main wave train is clearly visible and is followed by an incoherent coda. After averaging on the 123 realizations of disorder, the coherent field is obtained and is presented in figure 2(b). The main wave train is still clearly visible and all the incoherent variations of the field have greatly decreased.

With an incident P wave (respectively S wave), the coherent field is observed through the averaging of horizontal velocities u_x (respectively vertical velocities u_y). In such configuration, the propagation through the effective medium is equivalent to a 1D propagation in a slab, what explains that no effective S wave (respectively P wave) is observed in the case of an incident P wave (respectively S wave).

The dispersion curves and damping factor curves can now be estimated from the Fourier transform of this coherent field.

4 Signal processing

4.1 Methods

The phase velocity $c(\omega)$ is computed using the $p-\omega$ transform which represents the entire data wave field into the slowness-frequency domain ($p-\omega$), where $p = 1/c$ [8]. The method consists in a "slant stack summation" of the wave field (or $\tau-p$ transform, with τ representing a delay time) followed by a 1D Fourier transform over τ to obtain the wave field in the $p-\omega$ plane, where the dispersion curves can be directly picked. Here, we follow a formulation entirely in the frequency domain [9]. The time Fourier transform of the coherent field $s(\omega,d_i)$ at the distance d_i is

$$s(\omega,d_i) = A(\omega,d_i)\mathrm{e}^{-i\omega p_0(\omega)d_i}, \tag{4}$$

where $A(\omega,d_i)$ is the amplitude spectrum at d_i. The $p-\omega$ stack $\hat{s}(\omega,p)$ is

$$\hat{s}(\omega,p)=\sum_{i=1}^{N} A(\omega,d_i)e^{i\omega(p-p_0(\omega))d_i}. \tag{5}$$

The computation of $\hat{s}(\omega,p)$ is performed with several values of p. Given ω, the maximum of the modulus $|\hat{s}(\omega,p)|$ is reached at $p = p_0(\omega)$; the $|\hat{s}(\omega,p)|$ map is plotted as a 2D function of p and ω and the maximum locus is extracted at each frequency.

The damping factor is estimated from the decrease of the amplitude spectrum of the coherent field during propagation. In the frequency domain, the amplitude spectrum in (4)-(5) takes the following expression:

$$A(\omega,d_i) = A_0(\omega)\mathrm{e}^{-\alpha(\omega)d_i}, \tag{6}$$

where $A_0(\omega)$ is the amplitude of s at the first receiver. The damping parameter $\alpha(\omega)$ is determined by the slope of a least-square linear fit of $\ln(A(\omega,d_i))$. Since the incident wave is plane, no geometrical spreading has to be considered.

4.2 Analysis of accuracy

For evaluating the damping factor, no restriction is imposed about the number and position of receivers. For phase velocity, however, aliasing and limited resolution may be encountered [10]. The quantification of these artifacts has justified the numerical acquisition setup (number and position of the receivers). Aliasing occurs when $\Delta x_r > \lambda_{min}$, while resolution is limited by the total length of the acquisition setup $L_N = N \times \Delta x_r$. Phase velocity estimation is accurate as long as $\lambda < L_N/2$. Consequently, in the range of frequency under study, $L_N \geq 180$ mm and $\Delta x_r = 1$ mm.

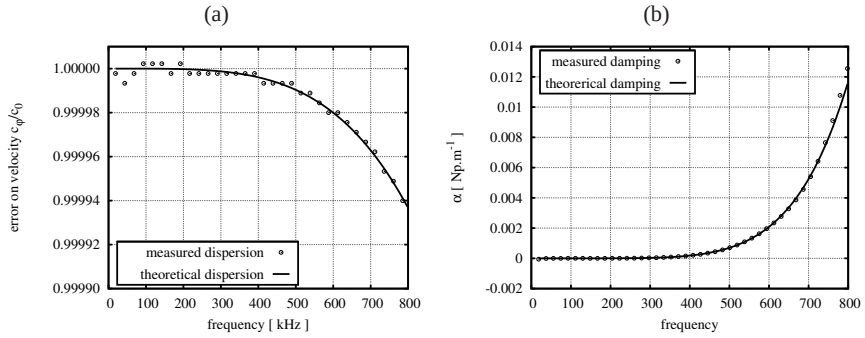

Fig. 3 1D homogeneous medium: analytical and simulated dispersion (a) and damping (b).

To evaluate how accurately the phase velocity and the damping factor are estimated, we apply the processing tools to 1-D simulation in an homogeneous medium, where numerical dispersion (2) and damping (3) are known. The numerical errors are maximum with the slowest celerity and shortest wavelength. In our case, it corresponds to the propagation of shear waves in mortar. A 1D homogeneous simulation of this case is computed, using the same numerical and acquisition parameters as used in 2D. The phase velocity and damping factor measured are compared to their theoretical counterparts in figure 3. The error between the theoretical curves and the measured ones is lower than 10^{-3}%. The signal processing method used and the acquisition setup chosen is then suitable to evaluate the dispersion curves and the damping factor with no significant signal processing artifacts.

5 Numerical experiments

5.1 Stabilized regime

The multiple-scattering regime requires a minimal distance of propagation to be established. The numerical tools proposed in sections 3 and 4 allow to estimate this distance l_{stab} to get a stabilized regime, frequently mentioned in the litterature [11] but rarely quantified to our knowledge. To do so, measures of α deduced from (6) are used: unlike the phase velocity, the attenuation may be estimated accurately on a distance of acquisition much smaller than the total length L_N, authorizing to test various zones of acquisition. Here, a fixed offset d_0 is considered, with a variable length of acquisition $L_M = d_0 + (M-1)\,\Delta x_r$ and $M \leq N$ (see section 3.3). The configuration under study is an incident S wave in a concrete C12.

Figure 4-(a) shows $\alpha(f)$ obtained with various values of the length of acquisition L_M. If $L_M < 90$ mm, the curves are noisy, especially in the low-frequency range where they do not grow monotonically, which is not realistic. In high frequency,

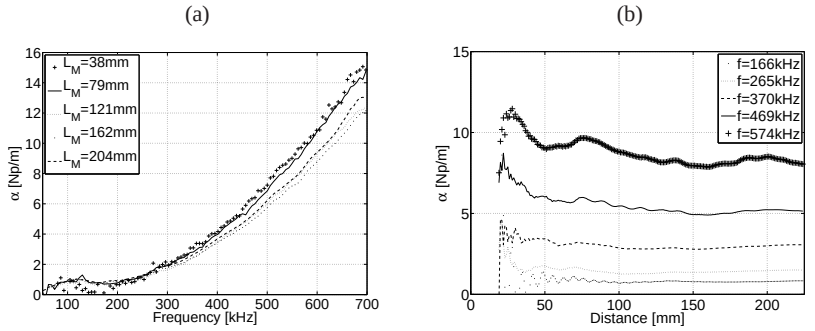

Fig. 4 Damping evaluated from the first offset d_0, at fixed length of acquisition L_M (a) and at fixed frequency (b).

differences up to 2 Np/m are measured between the various curves. Figure 4-(b) shows $\alpha(L_M)$ with various values of f. The attenuation is noisy up to $L_M \approx 90$ mm, independently of the frequency; with greater values of L_M, the curves are almost constant, which amounts to a stabilized regime of propagation.

This observation is confirmed with the other concentrations and with incident plane P waves. Only the approximate minimal length of acquisition L_M varies: 90 mm for C6, as seen in the previous paragraph; 70 mm for C12; and 50 mm for C18. These distances are close to $2\,l_\phi$ whatever the frequency range and the concentration.

Consequently, numerical simulations indicate that the minimal distance of propagation to get a stabilized scattering regime is roughly $l_{\text{stab}} \approx 2\,l_\phi$. Similar expressions have been proposed in the related area of band-gap creation in phonic crystals [12]. From now on, all measures are done by excluding this zone of stabilization, i.e. from $2\,l_\phi$ to L_N.

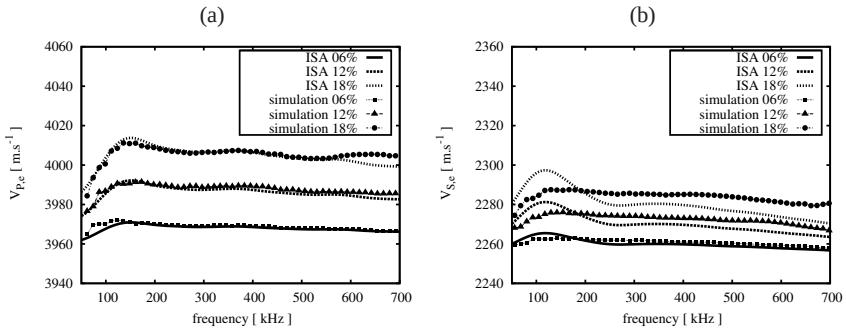

Fig. 5 Phase velocity: comparison between ISA and numerical simulations, with various concentrations of aggregates. (a): incident P wave (a); incident S wave (b).

5.2 Validity of ISA

The damping factor and phase velocity computed with ISA are compared to similar quantities measured on simulated data. The latter can be considered as the reference solutions, as shown in section 3.

First, the phase velocity is examined in figure 5. With an incident P wave (a), differences up to 1 m/s are observed between ISA and the simulated measures. Even with C18, ISA fits well the measured phase velocity. With an incident S wave (b), differences are of about 5 m/s, which remains acceptable. The slight decrease of the phase velocity at high frequencies is well described by ISA for both waves.

Second, the damping factor is examined in figure 6. With an incident P wave, the error is lower than 2 Np/m at the concentration 18 % (b). With an incident S wave, the same remark holds up to 12 %; with higher concentration, the error increases dramatically (d). In both cases, ISA gives better results with lowest concentration and low frequencies, which is consistent with the main hypotheses of a dilute medium.

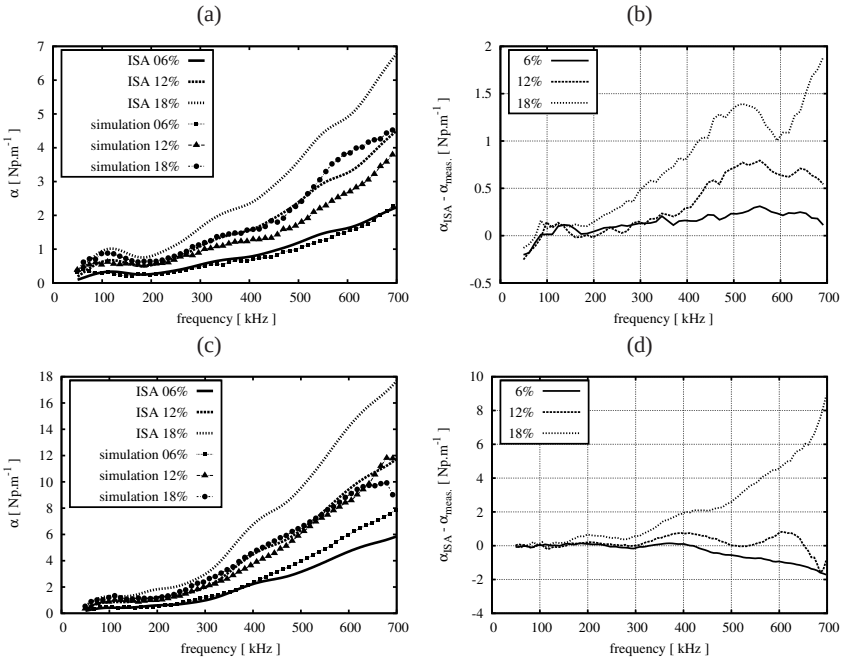

Fig. 6 Damping factor: comparison (left) and difference (right) between ISA and numerical simulations, with various concentrations of aggregates. Top: incident P wave; bottom: incident S wave.

6 Concluding remarks

The main results of this work are as follows:

1. the distance of propagation required to get a stabilized regime of multiple scattering is roughly $2\,l_\phi$, where l_ϕ is the mean distance between scatterers;
2. with an incident P wave, ISA provides good estimations of phase velocity and acceptable estimation of attenuation (lower than 2 Np/m) with a concentration nearly up to 20%; with an incident S wave, the concentration must be smaller than 10% to get the same agreement.

Three directions are distinguished for further investigation:

1. increasing the surfacic concentration of aggregates, up to 50%. Doing so requires to parallelize the algorithms used for direct numerical simulations;
2. considering continuous distribution size of aggregates, from a few mm to 20 mm. Is the aforementionned empirical formula still valid in the case of a medium where l_ϕ varies ?
3. studying higher-order multiple-scattering methods [11].

References

1. A. Derode, A. Tourin and M. Fink, *"Random multiple scattering of ultrasound. I. Coherent and ballistic waves"*, Phys. Rev. E 64, 036605, 2001.
2. M. Chekroun, L. Le Marrec, B. Lombard, J. Piraux and O. Abraham, *"Numerical methods for multiple scattering of ultrasound in random media"*, Proceedings of Waves 2007 Conference (Reading, UK), 2007, pp 492-494.
3. F. Schubert and B. Koehler, *Numerical time-domain simulation of diffusive ultrasound in concrete*, Ultrasonics **42**(1-9), 781-786 (2004).
4. A. Derode, V. Mamou and A. Tourin, *"Influence of correlations between scatterers on the attenuation of the coherent waves in random medium"*, Phys. Rev. E 74, 036606, 2006.
5. T. Schwartzkopff, M. Dumbser, C.D. Munz, *Fast high order ADER schemes for linear hyperbolic equations*, J. Comput. Phys., 197-2 (2004), 532-539.
6. J.S. Strikwerda, *Finite Difference Schemes and Partial Differential Equations*, Wadsworth-Brooks, New-York, 1989.
7. B. Lombard and J. Piraux, *Numerical treatment of two-dimensional interfaces for acoustic and elastic waves*, J. Comput. Phys., 195-1 (2004), 90-116.
8. G.A. McMechan and M.J. Yedlin, *"Analysis of dispersive waves by wave field transformation"*, Geophysics **46** (6), pp. 869-874 (1981)
9. T.A. Mokhtar, R.B. Herrmann and D.R. Russel, *"Seismic velocity and Q model for the shallow structure of the Arabian shield from short-period Rayleigh waves"*, Geophysics **53** (11), pp. 1379-1387 (1988)
10. T. Forbriger, *"Inversion of shallow-seismic wavefield: I. Wavefield transformation"*, Geoph. J. Int. **153**, 719-734 (2003)
11. C.M. Linton and P.A. Martin, *"Multiple scattering by random configurations of circular cylinders: second order corrections for the effective wavenumber"*, J. Acoust. Soc. America **117** (6), 3413-3423 (2005).
12. J-P. Groby, A. Wirgin and E. Ogam, *"Acoustic response of a periodic distribution of macroscopic inclusions within a rigid frame porous plate"*, Waves in Random and Complex Media (2008) - to be published